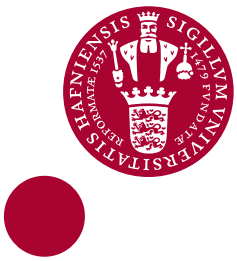

On the seawater temperature dependence of the sea spray aerosol generated by a continuous plunging jet

Salter, M.E.; Nilsson, E.D.; Butcher, Andrew Charles; Bilde, M.

Published in:
Journal of Geophysical Research: Biogeosciences

DOI:
10.1002/2013JD021376

Publication date:
2014

Document version
Publisher's PDF, also known as Version of record

AGU PUBLICATIONS

JGR

Journal of Geophysical Research: Atmospheres

RESEARCH ARTICLE

10.1002/2013JD021376

Key Points:
- Particle concentrations decreased as seawater temperature increased to ~9°C
- Bubbles with r_{film} < 2 mm decreased as seawater temperature increased to ~9°C
- Particle concentration was correlated with bubble density at the water surface

Correspondence to:
M. E. Salter,
matt.salter@itm.su.se

Citation:
Salter, M. E., E. D. Nilsson, A. Butcher, and M. Bilde (2014), On the seawater temperature dependence of the sea spray aerosol generated by a continuous plunging jet, *J. Geophys. Res. Atmos.*, *119*, 9052–9072, doi:10.1002/2013JD021376.

Received 20 DEC 2013
Accepted 11 JUL 2014
Accepted article online 15 JUL 2014
Published online 30 JUL 2014

The copyright line for this article was changed on 4 SEP 2014.

On the seawater temperature dependence of the sea spray aerosol generated by a continuous plunging jet

M. E. Salter[1], E. D. Nilsson[1], A. Butcher[2], and M. Bilde[3]

[1]Atmospheric Science, Department of Applied Environmental Science (ITM), Stockholm University, Stockholm, Sweden, [2]Department of Chemistry, University of Copenhagen, Copenhagen, Denmark, [3]Department of Chemistry, University of Aarhus, Aarhus, Denmark

Abstract Breaking waves on the ocean surface produce bubbles which, upon bursting, deliver seawater constituents into the atmosphere as sea spray aerosol particles. One way of investigating this process in the laboratory is to generate a bubble plume by a continuous plunging jet. We performed a series of laboratory experiments to elucidate the role of seawater temperature on aerosol production from artificial seawater free from organic contamination using a plunging jet. The seawater temperature was varied from −1.3°C to 30.1°C, while the volume of air entrained by the jet, surface bubble size distributions, and size distribution of the aerosol particles produced was monitored. We observed that the volume of air entrained decreased as the seawater temperature was increased. The number of surface bubbles with film radius smaller than 2 mm decreased nonlinearly with seawater temperature. This decrease was coincident with a substantial reduction in particle production. The number concentrations of particles with dry diameter less than ~1 μm decreased substantially as the seawater temperature was increased from −1.3°C to ~9°C. With further increase in seawater temperature (up to 30°C), a small increase in the number concentration of larger particles (dry diameter >~0.3 μm) was observed. Based on these observations, we infer that as seawater temperature increases, the process of bubble fragmentation changes, resulting in decreased air entrainment by the plunging jet, as well as the number of bubbles with film radius smaller than 2 mm. This again results in decreased particle production with increasing seawater temperature.

1. Introduction

Sea spray aerosol (SSA) is the key aerosol constituent over much of the Earth's surface and is therefore central to the description of its aerosol burden. Sea spray aerosols also exert an important influence on climate by scattering solar radiation and by serving as seed particles for cloud drops and ice crystals, affecting the microphysics and reflectivity of marine clouds and the development of precipitation.

Sea spray aerosol particles are formed predominately by the action of the wind on the ocean. Wind stress on the ocean surface forms waves, some of which break and entrain air into the ocean. The entrained air bubbles rise to the surface, create whitecaps, and burst. The result is injection of seawater drops into the atmosphere. Since the work of *Woodcock* [1953] which identified wind speed as the major driver of sea spray aerosol production, a series of studies attempting to relate aerosol concentration or production to local wind speed have followed [e.g., *O'Dowd and Smith*, 1993; *Nilsson et al.*, 2001].

Although the key meteorological factor governing the production of sea spray aerosol particles is the wind speed, the production flux of these particles may be affected by any meteorological or environmental factor that affects the surface properties of the ocean [*Lewis and Schwartz*, 2004]. The meteorological and environmental factors thought to be important in the process of sea spray aerosol production include seawater temperature (T_{sw}), sea ice coverage, absolute salinity (S_A), ocean wave field, and the chemical composition of the seawater, especially the presence of surface-active organic molecules.

It is very difficult to unambiguously separate and quantify the effects of the individual parameters. One approach to this problem has been laboratory experiments, and several approaches to entrain air and simulate whitecaps have been employed. Methods which continuously entrain air, such as a circular plunging jet of water or air forced through a frit below the water surface, have been utilized, as have discrete methods of air entrainment, such as the collision of two parcels of water. In the current study, we examine the effect

of seawater temperature on laboratory generated sea spray aerosol particles produced by a continuous circular plunging jet.

We begin with a brief bibliographic review of previous studies investigating the effects of seawater temperature on sea spray aerosol production processes. We then proceed to present a systematic experimental investigation of the effects of seawater temperature on plunging jet air entrainment, surface bubble size distributions, and sea spray aerosol production using a large-scale sea spray aerosol generation tank with stable temperature control. A list of the symbols used is provided as an appendix.

2. Previous Studies Concerned With the Effects of Seawater Temperature on Sea Spray Aerosol Production Processes

The effects of seawater temperature on sea spray aerosol production are likely manifold and relevant in processes from initial air entrainment to the final drop formation. The density (ρ_{sw}) and surface tension (γ_{sw}) of seawater change with temperature, but only by a fraction of a percent and a few percent, respectively, in the relevant range of absolute salinities (0 g kg^{-1} < S_A < 35 g kg^{-1}) and seawater temperatures (0°C < T_{sw} < 35°C) [*Sharqawy et al.*, 2010]. In contrast, seawater dynamic viscosity (μ_{sw}) decreases nonlinearly with increasing seawater temperature by a factor of ~3 from 0°C to 35°C [*Sharqawy et al.*, 2010]. Seawater temperature may affect bubble rise velocities, the rate of gas exchange between a bubble and the surrounding fluid, the subsequent number and size of bubbles arriving at the air-water interface, bubble bursting behavior, the drop formation process, and the oceanic whitecap fraction.

2.1. Whitecap Fraction

A series of studies have observed effects of seawater temperature on the fraction of the ocean surface covered by whitecaps (W); however, the findings often suggest complex relationships [*Wu*, 1979; *Monahan and Mac Niocaill*, 1986; *Monahan and O'Muircheartaigh*, 1986; *Bortkovskii*, 1987a, 1987b, 1997; *Wu*, 1988; *Bortkovskii and Novak*, 1993; *Stramska and Petelski*, 2003]. For example, *Bortkovskii* [1997] confirms the trend found in the laboratory by *Miyake and Abe* [1948] that the lifetime of whitecaps decreases as the seawater temperature increases but, at the same time, notes that whitecap fraction increases at higher temperatures.

Monahan and O'Muircheartaigh [1980] conducted the first substantial study to examine the potential effect of wind speed on whitecap fraction. They reported the most commonly used expression relating the whitecap fraction to wind speed:

$$W = 3.84 \times 10^{-6} \times U^{3.41} \tag{1}$$

where U is the wind speed (in units of m s^{-1}) at 10 m elevation. The data behind this model were obtained almost entirely in the sea surface temperature range 20°C to 30°C, and the authors noted that upon later inclusion of data obtained in the sea surface temperature range 12°C to 14°C, the model fit changed significantly (personal communication); for the same wind speed, the whitecap fraction was larger at lower temperatures than at higher temperatures.

The same authors came to similar conclusions when they considered a model based upon data obtained during the JASIN 1978 expedition (temperature range: 12.5°C to 14°C) [*Monahan et al.*, 1983]:

$$W = 5.4325 \times 10^{-6} \times U^{3.31} \tag{2}$$

This model results in ~20% higher values of W at U = 5 m s^{-1} and ~5% higher at 20 m s^{-1} when compared to equation (1). The authors speculated that the reason for this difference was the effect of seawater temperature on the rise velocity of bubbles in seawater (V_b) and the resulting effect on the lifetime of whitecaps. However, it is important to note that the data exhibited an immense amount of scatter, such that 20% differences are minuscule compared to the variability in the measurements themselves.

The possible dependence of whitecap fraction on seawater temperature was reviewed by *Lewis and Schwartz* [2004] who compared values of whitecap fractions obtained from 21 data sets across 11 studies. Data points were classified according to seawater temperature following *Bortkovskii* [1987a]: cold, T_{sw} < 4°C; intermediate, 4°C < T_{sw} < 17°C; and hot, 17°C < T_{sw}. The difference between whitecap fraction at cold and hot seawater temperatures from this analysis is striking. At higher seawater temperatures, the whitecap fraction appears considerably larger than that at low seawater temperatures for the same wind speed.

2.2. Bubble Concentrations and Size Characteristics

A number of studies have reported bubble concentrations and size characteristics as a function of seawater temperature. *Lessard and Zieminski* [1971] reported increasing bubble coalescence with increasing seawater temperature, using laboratory bubbles generated by capillary tips. *Asher and Farley* [1995] noted that the number of bubbles generated in the laboratory, using a tipping bucket mechanism at 15°C, was less than at 0°C, with the largest effect at the smallest bubble sizes. Using bubble clouds resulting from pressure-drop shattering of capillary generated bubbles, *Slauenwhite and Johnson* [1999] demonstrated that the number of bubbles produced through breakup of larger bubbles decreased with increasing seawater temperature. If applicable outside the laboratory, these findings would imply that decreasing bubble concentrations with increasing seawater temperature should occur. For example, the *Slauenwhite and Johnson* [1999] study would result in a decrease in total bubble concentration by at least 30% as the temperature of the seawater increased from 3°C to 20°C. A model incorporating the effects of seawater temperature on the size distributions of oceanic bubbles also suggested that bubble concentrations should decrease with increasing seawater temperature by ~7% per °C [*Thorpe et al.*, 1992]. Conversely, laboratory studies by both *Exton et al.* [1986] and *Pounder* [1986] found decreasing mean bubble size and increasing bubble concentrations with increasing seawater temperature. The contradictions across these studies are intriguing and suggest that factors other than solely seawater temperature were at play. For example, the results of these studies may have been affected by the presence of organic (surface active) material in the seawater used.

Most studies of bubbles in seawater report the bubble size distribution at some depth below the surface. The bubble size distribution evolves as it rises to the surface, and this evolution is indirectly affected by the temperature of the seawater: the terminal rise velocity of the bubbles is affected by the viscosity of the seawater. The effect is most pronounced at the smallest bubble sizes (volume equivalent bubble radius (r_b) <~0.06 mm). The terminal rise velocity of bubbles with volume equivalent bubble radius >~2.5 is affected very little by seawater temperature [*Lewis and Schwartz*, 2004].

2.3. Bubble Bursting

To understand the final process in the production of sea spray aerosol particles, knowledge of the size and number of drops formed by individual bursting bubbles at the water surface is critical. Two types of drops result from bursting bubbles: film drops, which form from fragments of the collapsed bubble cap, and jet drops, which form from the jet of water emitted following the collapse of the bubble cavity. The main factor controlling production of these two drop types is bubble size; however, seawater temperature is also a controlling factor via its effect on density, surface tension, and viscosity [*Lewis and Schwartz*, 2004]. The number of jet drops produced per bubble (N_{jet}) has been measured as a function of seawater temperature in a number of laboratory studies involving bursting of individual bubbles. A trend of decreasing jet drop number with increasing seawater temperature was observed [e.g., *Newitt et al.*, 1954; *Hayami and Toba*, 1958]. Fewer studies have examined the size of jet drops as a function of temperature. Both *Hayami and Toba* [1958] and *Blanchard* [1963] reported that jet drop size increased with increasing seawater temperature for all bubble sizes studied, while *Newitt et al.* [1954] observed the opposite trend. However, nearly all studies were conducted at a seawater temperature of 20°C and above, so conclusions relevant to the ocean as a whole cannot be drawn.

When considering the number of film drops produced per bubble (N_{film}), *Newitt et al.* [1954] found that increasing seawater temperature from 25°C to 45°C resulted in a decrease in N_{film} by a factor of approximately 2.5. Once again, the only real conclusion to be drawn from the studies conducted to date is that too little is known about film drop production to infer relationships between seawater temperature and the number and size of film drops produced per bubble [*Lewis and Schwartz*, 2004].

2.4. Simulating the Whole Process of Sea Spray Aerosol Production

Over the past few decades, a number of studies have simulated whitecaps, bubble bursting, and sea spray aerosol particle formation in the laboratory to simulate the entirety of the processes at play during sea spray aerosol production. A number of these studies have considered the effects of seawater temperature. A series of experiments conducted by *Woolf et al.* [1987] investigated the effect of seawater temperature on aerosol production in the temperature range 7.7°C to 23.4°C. Wave breaking was simulated through the collision of two parcels of seawater in the center of a tank (the same tank used by *Monahan et al.* [1982, 1983]). They found that production of particles with dry diameter (D_p) >~2.5 μm tended to increase with increasing seawater temperature. The temperature dependence was less apparent for production of particles with dry

diameter larger than 0.25 μm; there were sometimes large reductions in the number concentration of particles produced in this larger size range with increasing seawater temperature. In similar experiments, *Woolf and Monahan* [1988] noted that particle production was generally smaller at higher seawater temperatures for all particles with dry diameter larger than 0.25 μm.

Bowyer et al. [1990] used the same tank to study the effect of seawater temperature on sea spray aerosol in the temperature range 0°C to 30°C using local coastal seawater. Using a ROYCO model 225/519 particle counter, they presented the total number of aerosol particles larger than six specified size cuts. These size cuts were $D_p > 0.25$ μm, $D_p > 0.75$ μm, $D_p > 1.50$ μm, $D_p > 2.50$ μm, $D_p > 3.75$ μm, and $D_p > 5.00$ μm. While gradually increasing the seawater temperature, they identified a near-linear increase in number concentration with increasing seawater temperature in the four largest bins, with concentrations approximately doubling from 0°C to 30°C. However, when the two smallest size channels were included (thus, including all particles with $D_p >\sim 0.25$ μm), they observed a decrease in aerosol number by a factor of 3 when the seawater temperature increased from 0°C to 13°C and then very little change with further increase in seawater temperature. When the seawater temperature was increased rapidly, the aerosol number concentration increased all the way up to 20°C along with a lower nonlinear decrease, with further increase in seawater temperature, perhaps indicative of some form of hysteresis.

More than a decade later *Mårtensson et al.* [2003] reported effects of seawater temperature on the number of aerosol particles produced in the size range 0.02 μm $< D_p <$ 20 μm, using a differential mobility particle sizer and an optical particle counter. Measurements were made in a laboratory tank using artificial seawater at constant temperatures of −2°C, 5°C, 15°C, and 25°C and air entrainment provided by a submerged frit/diffuser. Particles with dry diameters as small as 0.02 μm (the lower limit of their measurements) were generated, and a dominant number mode (in the representation $dN_p/dlog(D_p)$) occurred at dry diameters near 0.1 μm.

Qualitatively, the results of *Mårtensson et al.* [2003] were similar to those of *Bowyer et al.* [1990] showing an increasing aerosol number concentration at large sizes and decreasing aerosol number concentration at smaller sizes with increasing seawater temperature. However, *Bowyer et al.* [1990] identified that these different trends crossed at a dry particle diameter of ∼1.5 μm, while *Mårtensson et al.* [2003] noted a crossing in the range 0.07–0.35 μm. The decrease in aerosol particle number concentration with increasing seawater temperature (in the range $-2°C < T_{sw} < 25$ °C) was about a factor of 3 in the small size range, and the increase in the larger sizes was about a factor 10. In the particle size range 0.07 μm to 0.35 μm, no clear trend was observed.

Sellegri et al. [2006] conducted laboratory experiments similar to those of *Mårtensson et al.* [2003] at seawater temperatures of 4°C and 23°C. They reported more particles with dry diameter smaller than 0.7 μm at 4°C relative to that at 23°C, and fewer particles at larger particle dry diameters. Qualitatively, their results were similar to those of *Mårtensson et al.* [2003] with higher aerosol number production for the smallest size range at the low temperature and vice versa for the largest particle range.

Hultin et al. [2011] performed laboratory tank experiments, where the tank seawater was continuously replaced with locally sourced shallow Baltic Sea waters. In contrast to the laboratory experiments of *Mårtensson et al.* [2003], a plunging water jet was used to entrain air instead of a glass filter/diffuser. They found that total sea spray aerosol particle production decreased with increasing temperature of the seawater in the range 10.3°C to 17.4°C. The authors related the observed temperature dependence to variation in diurnal cycles in the marine microbiological respiration. However, during the same study, they also conducted an off-line experiment, where the seawater temperature was increased from 4°C to 18°C. Similar to their previous experiments, the sea spray aerosol number production decreased with increasing seawater temperature in all sizes (dry diameters from 0.02 μm to 1.8 μm). This suggests that the observed decrease in particle production may have been a physical rather than biological effect. In addition, the temperature dependence was nonlinear, with most of the reduction in production occurring in the temperature range 4°C to 12°C. The change in sea spray aerosol production over this temperature range was larger than reported by both *Bowyer et al.* [1990] and *Mårtensson et al.* [2003], by approximately a factor of 5.

Zábori et al. [2012a] conducted similar laboratory experiments using Arctic Ocean seawater that was either cooled from room temperature to close to its freezing point or heated back up from this temperature to close to room temperature. The difference between this study and some of those described previously

[e.g., *Mårtensson et al.*, 2003] was that the seawater temperature was continuously changing (increasing or decreasing) while in the previous studies it was held constant. The continuous change in seawater temperature might have resulted in supersaturation of atmospheric gases during the heating experiments and undersaturation during the cooling experiments. The effects of gas saturation on sea spray aerosol particle production are unclear [e.g., *Stramska et al.*, 1990; *Thorpe et al.*, 1992], but qualitatively, the results were similar to *Hultin et al.* [2011], showing a nonlinear decrease in sea spray aerosol particle production for all particle sizes with increasing seawater temperature and largest effects at seawater temperatures lower than 9°C. Changes in aerosol production with temperature were once again larger than observed by both *Bowyer et al.* [1990] and *Mårtensson et al.* [2003] (by a factor of between 3 and 6). A follow-up experiment using an identical setup and water containing either pure NaCl (15 g kg^{-1} to 35 g kg^{-1}) or NaCl spiked with succinic acid (0 μmol l^{-1} to 94 μmol l^{-1}) exhibited similar results [*Zábori et al.*, 2012b].

There is a clear difference in the observed magnitude of the seawater temperature effects on sea spray aerosol production between experiments deploying glass filters/diffusers [e.g., *Mårtensson et al.*, 2003; *Sellegri et al.*, 2006] and experiments using plunging water jets [e.g., *Hultin et al.*, 2011; *Zábori et al.*, 2012a, 2012b] despite the similar trends. The experiments using plunging jets yield results most similar to those of *Bowyer et al.* [1990]. This might be because there are similar bubble size distributions in those experiments using plunging jets and studies with plunging waves/colliding water parcels such as that conducted by *Bowyer et al.* [1990].

To summarize, effects of seawater temperature on sea spray aerosol production fluxes have been noted in real and artificial seawater, at different salinities and in water containing different organic species at different concentrations. However, it appears that experiments operating at steady state and those testing dynamic temperature changes result in different temperature dependencies. In this work, a laboratory tank with improved temperature control over long time periods was constructed with the purpose of obtaining new insight into the physics behind the dependence of the sea spray aerosol production flux on seawater temperature.

3. Methods

3.1. Sea Spray Simulator

To examine the effect of seawater temperature on sea spray aerosol particles generated using a laboratory continuous plunging jet, a large volume sea spray simulator was constructed (Figure 1). The system was fabricated from stainless steel components and consisted of a jacketed stainless steel vessel (hereafter referred to as "the tank"). The jacket section was plumbed to a temperature controlled ($\pm$0.1 k) water circulating bath (Grant, LTC1) containing 30% glycol. To avoid leaching of organics from moving parts, seals, and glands, a peristaltic pump (Watson-Marlow, 620S) was used to generate the plunging jet by pumping water from the center of the tank bottom back through the center of the lid. Inside the tank a stainless steel nozzle with inner diameter 4.3 mm (Swagelok Stainless Steel Fractional tube adapter; SS-400-R-4) held in a vertical position 30 cm above the air-water interface was used as the exit for the plunging jet.

All surfaces below the water level on the inside of the tank were coated in polytetrafluoroethylene (PTFE), and all tubing in contact with sample water was made of silicone. A series of ports along the side and top of the tank allowed for sampling of water and air, respectively. Prior to all experiments, all internal surfaces were rinsed thoroughly with low-organic-carbon, $>$ 18.2 MΩ resistivity, Type 1 American Society for Testing and Materials standard, deionized water. The inner diameter of the tank was 47 cm, the depth was 60 cm, and wall interactions with the bubble plume, generated by the plunging jet, were assumed negligible. Table 1 summarizes the dimensions and operating conditions of the tank.

Dry zero sweep-air entered the tank at 6 l min^{-1} after passing through an ultrafilter (Type H cartridge, MSA) and an activated carbon filter (Ultrafilter, AG-AK). The airflow rate was maintained and quantified using a mass flow controller (Brooks, 5851S). Aerosol-laden air was sampled through a port in the lid of the tank and transferred under laminar flow conditions to the connected aerosol instrumentation. To prevent contamination by room air, the tank was operated under slight positive pressure by maintaining the sweep-air flow several liters per minute higher than the sampling rate. Excess air was vented through a one-way flutter valve on the lid of the tank.

Both seawater salinity and temperature were measured continuously using an Aanderaa 4120 conductivity sensor. The concentration of dissolved oxygen in the seawater was measured with an Aanderaa oxygen

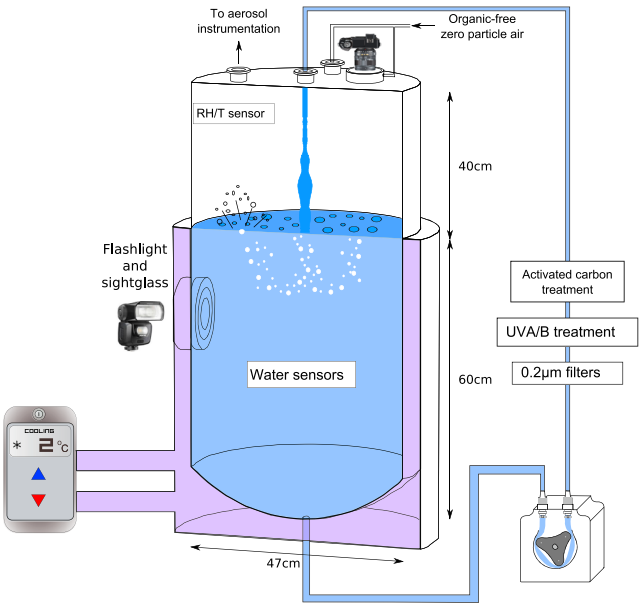

Figure 1. Schematic of the plunging-jet tank constructed for the experiments.

optode 4175. This sensor also provided an independent temperature measurement. Both sensors were placed toward the center of the tank, approximately halfway between the tank base and the air-water interface. Relative humidity and temperature were measured in the headspace of the tank using a Vaisala model HMT333 probe.

3.2. Air Entrainment by Plunging Jets

Having introduced the sea spray simulator used in this study, it is pertinent to consider the process of air entrainment by plunging jets and how it relates to the process of air entrainment in breaking waves at the ocean surface. Air entrainment at a continuous plunging jet is a function of the inflow conditions as well as the jet dimensions [*Cummings and Chanson*, 1999]. Jet properties important for air entrainment include the jet velocity at impact, the physical properties of the fluid, the jet nozzle design, the length of the free-falling jet, and the jet turbulence.

A number of reviews on air entrainment by plunging jets have been conducted [e.g., *Bin*, 1993; *Chanson*, 1997; *Kiger and Duncan*, 2012]; however, understanding of air entrainment processes remains limited. In the context of laboratory sea spray aerosol studies, two major points should be borne in mind. First, it is important to consider the fluid properties. *Chanson et al.* [2006] reported that less air was entrained in seawater compared to tap water, which they attributed to diminished air entrapment at impingement in the seawater due to the presence of natural surfactants. This implies that the surface tension of the fluid is likely to be important for air entrainment. Further, surface tension has also been shown to affect energy dissipation by small-scale laboratory breaking waves [*Stagonas et al.*, 2011].

Second, the ratio of important factors (e.g., gravity and surface tension) in the plunging jet experiments should be as close as possible to the prototype of breaking waves, such that dynamic similarity between plunging jets and breaking waves can be achieved. Unfortunately, this is impossible with geometrically similar models because of the large number of relevant dimensionless parameters. This leads to scale effects and means that laboratory scale models cannot be directly compared with the prototype of breaking waves [*Chanson*, 1997].

Table 1. The Dimensions and Operating Conditions of the Tank

Characteristic	Value
Inner diameter (cm)	47
Cross section (cm^{-2})	1735
Seawater depth (cm)	60
Seawater volume (l)	104
Headspace depth (cm)	40
Headspace volume (l)	69
Zero sweep-air (l min^{-1})	6
Headspace residence time (assuming perfect mixing) (min)	11.5
Plunging jet flow rate (l min^{-1})	1.73
Seawater velocity at nozzle exit (m s^{-1})	2.29
Seawater velocity at the free water surface (m s^{-1})	3.62

3.3. Aerosol Measurements

Aerosol-laden air was directed through 2 m of 0.5 inch stainless steel tubing and two silica diffusion driers (TSI Model 3062) at which point the flow was split. Immediately following this split, a GRIMM 1.109 optical particle counter was used to measure particles with $D_p > 0.25$ μm. The aerosol size distribution in the size range 0.25 μm $< D_p < 32$ μm was determined every 6 s, sizing particles in 31 bins. The second sampling line was directed to an instrument payload where the flow was split further. One sampling line was

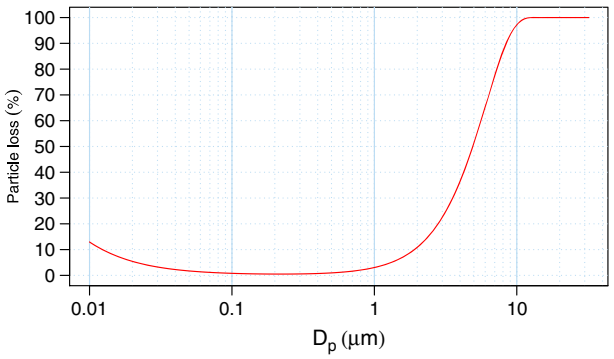

Figure 2. Calculated particle losses for the length of tubing between the tank and the inlet to the differential mobility particle sizer/scanning mobility particle sizer/optical particle counter instruments based upon the procedure in *von der Weiden et al.* [2009]. Losses were calculated based upon a particle density of 1000 kg m^{-3} with a shape factor of 1.

directed to a TSI model 3772 condensation particle counter to measure the total number concentration of particles with $D_p > 0.01$ μm at a frequency of 1 Hz. The other sampling line passed through an impactor (TSI Model 1035900, 0.0707 cm nozzle, D50 cutoff = 1 μm at 1 l min^{-1}) before entering a closed-loop sheath air, custom-built differential mobility particle sizer (DMPS) (selecting negatively charged particles) connected to a condensation particle counter (TSI model 3772). This setup was used to determine the size distribution in the size range 0.01 μm $< D_p <$ 0.41 μm, and a single scan over 34 size bins was completed in 11 min. All data logging as well as the data inversion was conducted with custom-built software.

A TSI 3936 scanning mobility particle sizer system (SMPS), consisting of a long differential mobility analyzer (TSI 3080L) and a TSI 3010 condensation particle counter, was also used to measure particle size distributions in the size range 0.01 μm $< D_p <$ 0.7 μm for a subset of the experiments. This system was used with the TSI AIMS software package for data inversion. Prior to entering the system, the aerosol sample was first passed through the same impactor as used in the differential mobility particle sizer system. The scanning mobility particle sizer system selected negatively charged particles (modified from the standard configuration through the use of a positive high-voltage power supply to the differential mobility analyzer). A single scan over 109 size bins was completed in 5.5 min. Both differential mobility analyzers were operated with recirculating sheath air.

Particle losses in the sizing instrument sampling lines and diffusion driers were calculated based upon the procedure in *von der Weiden et al.* [2009], assuming a particle density of 1000 kg m^{-3} and a shape factor of 1. The particle density refers to the mass per unit volume of the particle itself, not of the aerosol, the "density" of which we refer to as concentration. For particles with $D_p < 2$ μm, losses were below 10%; however, losses increased to $>$ 50% for particles with dry diameter $>$ 5 μm (Figure 2). Given that we have the capability to size particles up to 32 μm, these losses are high. However, it became apparent during the measurement campaign that drying the aerosol prior to measurement was not trivial and that in order to ensure we were actually measuring dry particle sizes, we would have to forgo measurement of larger ($\sim$>2 μm dry diameter) particles because of the large losses. We nevertheless report our measured values using the optical particle counter, but the reader should bear these losses in mind. It should also be noted that these loss calculations only indicate the approximate magnitude of the losses in our sample lines. Therefore, to avoid the inclusion of added uncertainty, we have not corrected the aerosol data we present for these losses. Given that we have significant losses of larger particles in our system, it is not unfeasible that we were only able to observe the effect of the seawater temperature increase on the smaller particles and that any effect on the larger particles [e.g., *Mårtensson et al.*, 2003; *Bowyer et al.*, 1990] (see section 2.4 for discussion) was masked by these losses.

The temperature and relative humidity of the sampled air as well as the sheath air of the differential mobility analyzers were monitored using a Campbell Scientific HMP50 sensor.

3.4. Experimental Setup

Each experiment was conducted with artificial seawater (hereafter referred to as seawater) consisting of sea salts (Sigma Aldrich, S9883) rehydrated to an absolute salinity of 35 g kg^{-1} using deionized water. The composition of the sea salt by mass was as follows: 55% Cl^-, 31% Na^+, 8% SO_4^{-2}, 4% Mg^{+2}, 1% K^+, 1% Ca^{+2}, $<$ 1% other.

Artificial seawater free from organic contamination is difficult to obtain; contamination is often large enough that artificial seawater exhibits an adsorption spectrum nearly identical to that of filtered (0.2μm) seawater obtained from oligotrophic seawater [e.g., *Twardowski et al.*, 1999]. We therefore subjected our

Table 2. Summary of Experimental Phase One[a]

		Seawater					Headspace		Inlet
Experiment	Duration (h)	T_w (°C)	O_2 %	ρ_{sw}[b] (kg m^{-3})	μ_{sw}[b] (g m^{-1}s^{-1})	γ_{sw}[b] (N m^{-1})	T (°C)	RH (%)	RH (%)
1	6.1	−1.3	112	1028.0	1.99	0.0764	8.9	91	11
2	6.8	−0.5	115	1028.0	1.94	0.0763	9.3	93	12
3	6.5	0.5	115	1028.0	1.87	0.0761	10.0	91	13
4	6.0	1.4	114	1027.9	1.82	0.0760	9.5	93	14
5	6.4	2.3	114	1027.8	1.76	0.0759	10.3	92	15
6	6.3	3.2	114	1027.8	1.71	0.0758	11.0	91	12
7	7.9	4.1	113	1027.7	1.67	0.0757	11.5	92	14
8	6.2	5.1	113	1027.6	1.61	0.0755	12.0	92	15
9	6.2	6.1	113	1027.5	1.57	0.0754	13.1	91	16
10	8.8	7.9	112	1027.3	1.48	0.0752	12.9	94	19
11	8.9	9.9	112	1027.0	1.40	0.0749	13.7	95	16
12	5.5	15.0	111	1026.1	1.22	0.0742	17.3	96	21
13	6.4	20.1	111	1024.9	1.07	0.0735	20.6	97	19
14	6.0	30.1	113	1022.0	0.86	0.0721	28.5	100	26

[a]All experiments were conducted at a salinity of 35 g kg^{-1} (the same seawater was used for all experiments) with a plunging jet flow rate of 1.73 l min^{-1}. RH stands for relative humidity, and O_2 is the % saturation of oxygen in the seawater.

[b]Calculated using the equations given in *Sharqawy et al.* [2010].

artificial seawater to a purification process consisting of activated charcoal treatments, artificial UV exposures and hydrogen peroxide (H_2O_2, 30% solution, no stabilizer) additions. Here H_2O_2 acted as an oxidizing agent to remove organic matter.

Prior to the first experiment, H_2O_2 was added to the artificial seawater at a concentration of 20 mg l^{-1}. The tank was then sealed to the atmosphere and continually flushed with zero sweep-air (6 l min^{-1}). A tubular, ultraviolet, electromagnetic radiation subtype C (0.100μm to 0.280μm) reactor (Deltec T5) with a central low-pressure 80 W mercury lamp contained within a quartz sleeve was inserted in the peristaltic pump-plunging jet circuit inline with a 0.2μm Whatman Polycap filter and a Whatman inline Carbon filter. Finally, the peristaltic pump was switched on and operated continuously (flow rate 1.73 l min^{-1}) for $>$ 24 h. During this process, the consumption of H_2O_2 in the seawater was monitored using Quantofix (Macherey-Nagel) peroxide test strips covering the range 1 mg l^{-1} to 100 mg l^{-1}. Once values of H_2O_2 were below the detection limit of the method (1 mg l^{-1}), the UV reactor was switched off and removed from the peristaltic pump-plunging jet circuit along with the filters, and the first experiment was started.

Two phases of experiments were conducted to investigate the influence of seawater temperature on aerosol production by the plunging jet. During the first phase, the seawater temperature was varied while measurements of the size distribution of the surface bubbles and aerosol particles generated were conducted. The second phase of the experiment consisted of measurements of air entrainment by the plunging jet, while the seawater temperature was varied across the same range as during the first phase of experiments. This second phase was conducted 24 h after the first phase of experiments had ended, since it involved the construction of a stainless steel column around the jet. The tank was kept closed with a constant inflow of zero-particle air during the interim period, and the same seawater was used during both phases of experiments.

During both experimental phases, the seawater temperature was varied from −1.3°C to 30.1°C in increments of 1°C in the range −1.3°C to 8.1°C and in increments of 5°C thereafter. Each experiment was conducted at constant temperature over a period of at least 5 h (Table 2), following a period of at least 12 h at the desired temperature. This was to ensure that dissolved gas molecules were in thermodynamic equilibrium (~100% saturation) with the gas phase in the headspace of the tank. Measurements of oxygen concentration in the seawater confirmed this to be the case, and the oxygen % saturations were not significantly different between the experiments (Table 2). The mean oxygen saturation across all experiments was 113% with a standard deviation of 1% (the reported accuracy of the Aanderaa oxygen optode 4175 is to within $<$ 5% saturation). The significant supersaturation that we observed results from the increase in hydrostatic pressure inside the entrained bubbles (due to their depth) as well as their surface tension. Although

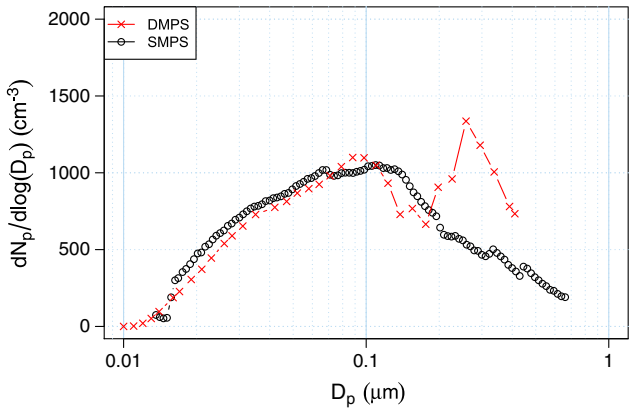

Figure 3. Mean aerosol number size distributions measured at a seawater temperature of 9.9°C using the differential mobility particle sizer (red line and crosses) and scanning mobility particle sizer (black line and circles) systems.

this oxygen saturation anomaly is high, it is within the range of anomalies typically encountered in ocean surface waters [*Najjar and Keeling*, 1997].

The relative humidity of the aerosol at the inlet to the instrumentation was always below 26% (Table 2). Therefore, we assume that all particles had effloresced and we report our measured particle diameters as dry diameters (D_p).

3.5. Particle Size Distributions

Dry particle size distributions were first obtained using the differential mobility particle sizer system, covering the dry diameter size range 0.01μm to 0.41μm, and the optical particle counter, covering the dry diameter range 0.25μm to 32μm. Rather than a direct particle number size distribution, the differential mobility particle sizer measures an electrical particle mobility distribution which, given knowledge of the bipolar charge distribution [*Wiedensohler*, 1988] and the instrument responses of the differential mobility analyzer and particle counter, can be inverted to yield the size distribution [*Alofs and Balakumar*, 1982; *Kandlikar and Ramachandran*, 1999]. However, if no impactor is installed in front of the differential mobility analyzer column or if the cutoff size of an installed impactor is larger than the upper size range in the size scan, multiply charged particles larger than the uppermost size in the scan can result in artifacts in the inferred particle size distribution because they are not accounted for in the multiple charge inversion.

Sea spray aerosol contains a significant number of particles outside the differential mobility particle sizer range. The red line in Figure 3 plots the full size distribution obtained using the custom-built differential mobility particle sizer (0.01μm to 0.41μm dry diameter) at 9.9°C. In the representation $dN_p/dlog(D_p)$, the size distribution appears bimodal with number concentration maxima around 0.1μm and 0.260μm dry diameter. In comparison, the size distribution measured with the scanning mobility particle sizer system (size range: 0.14μm and 0.660μm dry diameter, Figure 3, black line) appears unimodal with a single concentration maximum around 0.100μm. The smaller difference between the impactor cutoff size and the uppermost bin of the scanning mobility particle sizer system compared to the difference between the impactor cutoff and the uppermost bin of the differential mobility particle sizer system results in fewer artifacts from multiply charged particles.

The predicament of multiply charged particles may well have been an issue in previous laboratory plunging jet sea spray experiments, when either an impactor was not used (or not stated) or the particle sizer had an upper cutoff significantly lower than the cutoff of the impactor used [e.g., *Sellegri et al.*, 2006; *Hultin et al.*, 2010, 2011; *Zábori et al.*, 2012b, 2012a, 2013]. We expect such problems to be largest when particle generation is induced by a plunging jet because aerosol production by forcing air through a frit below the water surface typically results in a smaller proportion of large particles than aerosol production by a plunging jet.

Since the scanning mobility particle sizer system was only used at three of the temperatures investigated (−1.3°C, 9.9°C and 30.1°C), in the following we discuss only the differential mobility particle sizer data given that they span the whole temperature range at high resolution. To avoid artifacts from the multiple charging issues discussed above, we have calculated the uppermost differential mobility particle sizer sampling channel (0.176μm) deemed to be unaffected by double- and triple-charged particles based upon the largest sampling channel of 0.410μm and have removed all sample channels larger than this from further analysis. Given that the scanning mobility particle sizer data suggest that the particle size distribution is unimodal and the remaining sampling channels in the differential mobility particle sizer encompass the maxima of this mode, we deem this to be a reasonable approach.

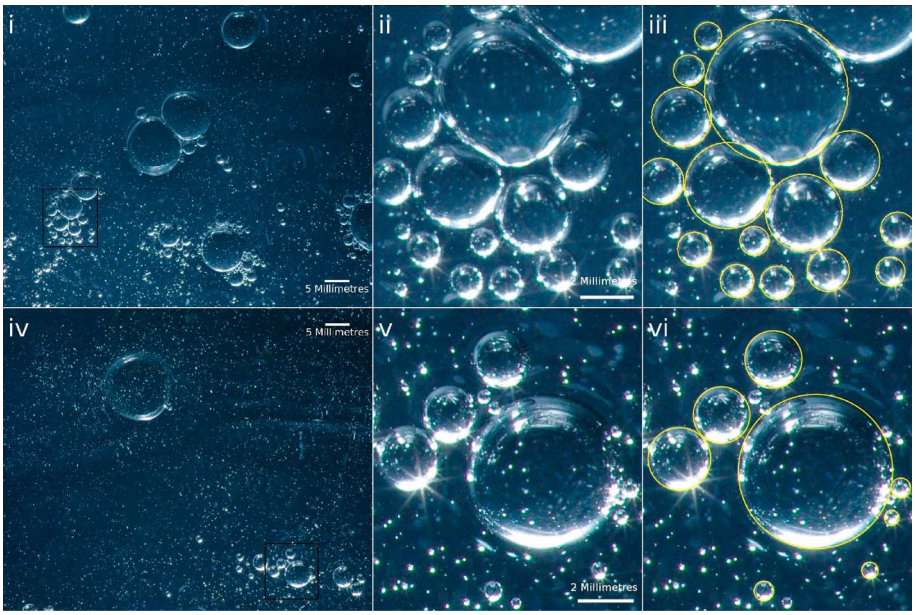

Figure 4. Full size digital images of the water surface at (i) −1.3°C (Experiment 1) and (iv) 30.1°C (Experiment 14). Images (ii) and (v) are zoom images of the rectangles highlighted in images (i) and (iv), respectively. Images (iii) and (vi) show the circles fit to these bubbles.

The measurement of particle size with an optical particle counter, such as the one used in this study, is based on the assumption that the scattered light intensity is a monotonic function of particle size. However, the optical particle counter response depends not only on particle size but also on sphericity and the refractive index of the particles. Since the aerosol particles produced in this study have an unknown sphericity and refractive index, the error in size estimation might be significant. However, we have used the same composition of sea salt throughout our study, and thus, it seems reasonable to assume that the size distributions obtained under different conditions can be directly compared. Since the optical particle counter was used with calibration parameters preset by the supplier, we assume that the aerosol particles we measured were spherical and that their index of refraction was the same as the particles used for the instrument's calibration (polystyrene latex (PSL) spheres, with a refractive index of $1.59-0i$). In comparison, NaCl has a refractive index of $1.54-0i$. Measurement of non-PSL aerosols such as sea salt aerosol particles with an optical particle counter factory calibrated with PSLs will manifest in a diameter shift of the size distribution due to differences in the refractive index of the materials. Given that the optical particle counter was sizing particles over a large range of particle sizes ($0.25\mu m < D_p < 32\mu m$), "Mie ambiguities" will have occurred. However, according to the instrument's manual, no smoothing algorithms were applied in order to account for these and we have made no attempt to correct for them.

The optical particle counter used during the study counted particles with dry diameters in the range $0.25\mu m$ to $32\mu m$; however, the counting efficiency of the instrument is not constant across this range. Instead, it exhibits a counting efficiency which decreases from ~100% above $0.780\mu m$ to approximately 90% at $0.305\mu m$ before decreasingly steeply below $0.305\mu m$ [*Heim et al.*, 2008]. Therefore, we present only data obtained in the sampling channels above $0.300\mu m$ in the subsequent analysis.

3.5.1. Bubble Photoregistration and Size Measurements

To determine the bubble size distribution at the water surface, the bubbles were photographed at 60 s time intervals, from 40 cm above the water surface (measured from the front lens element of the camera lens), and approximately 10 cm from the centerline of the plunging jet, using a Pentax K-7 Digital Single Lens Reflex camera (DSLR) equipped with a SMC Pentax-DFA Macro 100 mm F/2.8 lens macro lens capable of 1:1 reproduction.

The aperture was closed to F/11 to increase the focal depth, and the lens was automatically focused on the water surface. The bubbles were backlit by placing a Pentax AF-540FGZ flashlight adjacent to a submerged viewing window. This arrangement provided enough light near the water surface to distinguish the bubbles against a dark background (Figure 4).

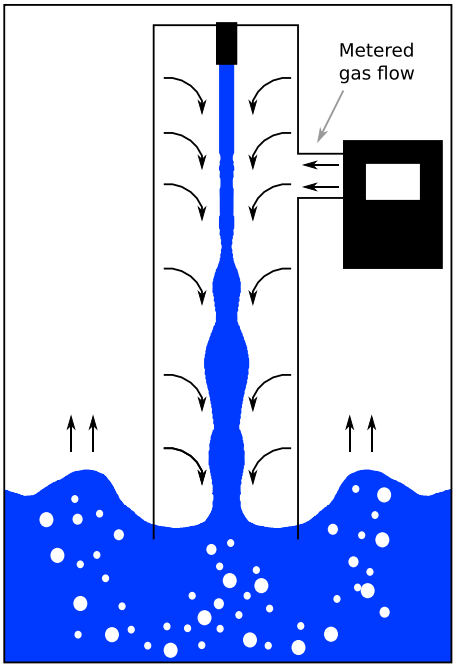

Figure 5. Schematic of the apparatus used to measure air entrainment in the tank.

The camera and the flash were tethered to a computer using the PK-Tether software. Bubbles were manually identified in each image, and a circle was fitted to each bubble using the ImageJ software [*Schneider et al.*, 2012]. The 60 s time interval was chosen to ensure that the same bubbles were not counted more than once.

The camera captured 3104 × 4672 pixel images which represented a 61 × 92 mm section of the water surface. This was based on a sensor size of 15.6 × 23.4 mm and an empirically derived scaling factor: The macro lens has a scale of 1:1 when at the minimum focal distance; however, at 40 cm distance, as was the case during our experiments, the reproduction scaling was determined to be 1:3.9. The major axis of each circle identified by ImageJ was subsequently exported to a text file for further analysis.

It is important to note that most references to bubble size distributions in the literature refer to the volume equivalent radius of the bubble if it was spherical (r_b). This is because nearly all existing studies refer to subsurface bubbles which are approximately spherical. However, a bubble resting in equilibrium at the surface of a liquid is not spherical. Instead, the intersection of this bubble film with the water surface forms a circle with a radius known as the bubble film radius (r_{film}) [*Lewis and Schwartz*, 2004, Figure 31]. It is this circle that the photographs captured during this study (Figure 4).

Based on the pixel size and resolution of the camera sensor and the influence of lens diffraction, the minimum discernable bubble film radius was estimated to be 0.02 mm. However, at bubble film radii smaller than 0.25 mm, it became increasingly difficult to differentiate bubbles at the surface from those in the subsurface; therefore, bubbles with bubble film radii smaller than 0.25 mm were not included in the subsequent analysis.

Table 3. Summary of Experimental Phase Two[a]

			Rate of Air Entrainment[b]	
Experiment	T (K)	P (hPa)	Mean ($cm^3 min^{-1}$)	1σ ($cm^3 min^{-1}$)
1	272.0	1008	2458	89
2	272.1	1008	2434	86
3	272.7	1008	2447	109
4	273.7	1009	2413	80
5	275.2	1009	2391	84
6	277.2	1009	2388	66
7	278.2	1009	2374	66
8	280.3	1010	2338	102
9	281.8	1010	2304	74
10	283.6	1011	2297	78
11	288.0	1014	2156	67
12	293.7	1015	2081	61
13	298.6	1015	2046	43
14	303.1	1015	1971	48

[a]All experiments were conducted at a salinity of 35 g kg^{-1} (the same seawater was used for all experiments) with a plunging jet flow rate of 1.73 l min^{-1}.

[b]On the basis of 30 measurements uncorrected for T and P.

3.5.2. Measurements of Air Entrainment

Air entrainment was measured by modifying the plunging jet as shown in Figure 5. A stainless steel column enclosed the entire length of the plunging jet. The top of the column was welded to the base of a nozzle identical to that used during the aerosol measurements, and the base of the column was submerged in the water to a depth of approximately 10 mm below the free surface of the water. Thus, air could enter the column only through a metered inlet toward the top of the column, which was open to the atmosphere. The jet was aligned with the vertical axis of the column so that the liquid jet plunged into the water below.

At each temperature of interest, the entrained air volumetric flow rate was recorded 30 times using a low-pressure-drop Gilibrator volumetric flow meter (Gilian, West Cladwell, NJ). The measured air volume entrainment rate of these 30 measurements was then averaged and corrected to a standard temperature and

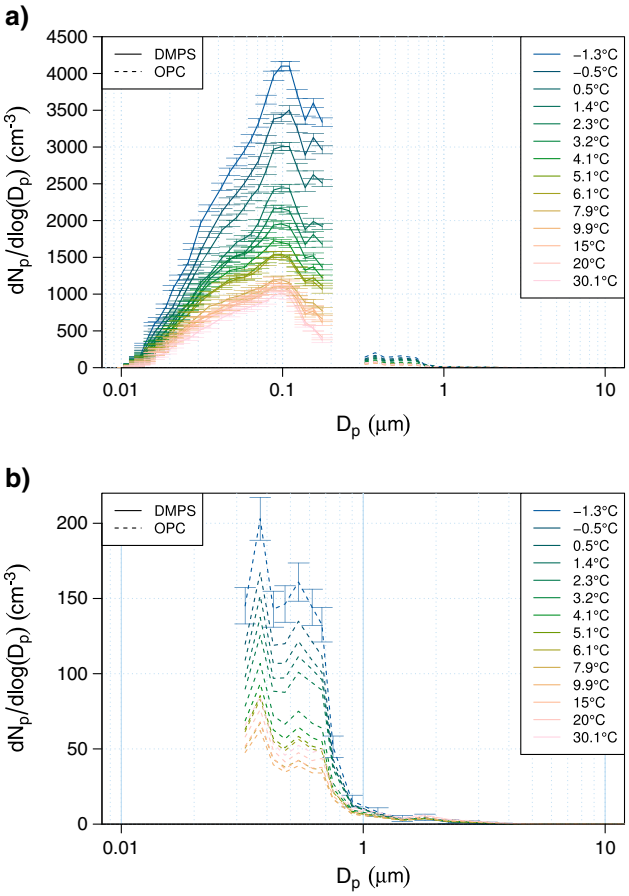

Figure 6. (a) Mean aerosol number size distributions (error bars represent 1σ) measured at all seawater temperatures investigated and (b) the same plot with axes scaled to highlight the optical particle counter data. In this panel, error bars are omitted for clarity for all temperature experiments except that of the coldest seawater where they were at their highest.

pressure by multiplication with $298.15/T$ and division by $P/1013.25$, where T was the air temperature in the stainless steel column surrounding the jet in Kelvin, and P was the air pressure in hPa. Since it was not possible to measure T directly due to the very small distance between the plunging jet and the stainless steel column (~5 mm), we have assumed it was equal to the temperature of the seawater in the plunging jet. Table 3 summarizes the details of the air entrainment experiments.

4. Results

4.1. Particle Size Distributions

The effect of the seawater temperature on the magnitude and the shape of the aerosol number size distribution is shown in Figure 6. Upon initial inspection, there are two local maxima, one at a dry diameter of 0.100μm and the other at a dry diameter of 0.375μm. Figure 7 reveals that the relative proportion of these two maxima changes as a function of seawater temperature. The number of particles at a dry diameter of 0.100μm is influenced more strongly by changes in seawater temperature than the number of particles at a dry diameter of 0.375μm. The data shown in Figure 7 are fitted moderately well by a linear expression (coefficient of determination, $R^2 = 0.87$; P-value $= 6.8 \times 10^{-7}$).

4.2. Particle Number Concentration

The number concentration of particles with dry diameter larger than 0.01μm measured using the TSI 3772 condensation particle counter and of particles with dry diameter larger than 0.3μm measured by the GRIMM 1.109 optical particle counter as a function of seawater temperature is presented in Figure 8. Particle concentrations in both size ranges show strong nonlinear decreases as the seawater temperature is increased from −1.3°C to 9.9°C. Between 9.9°C and 30.1°C, the concentration of particles larger than a dry diameter of 0.01μm remains relatively constant, while the concentration of particles larger than a dry diameter of 0.3μm appears to increase slightly with increasing seawater temperature.

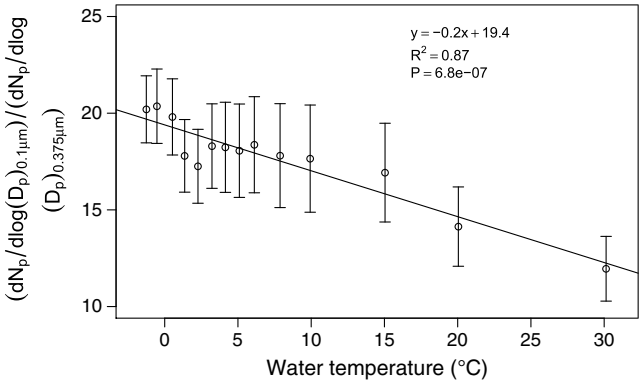

Figure 7. Ratio of $dN_p/dlog(D_p)_{100nm}/dN_p/dlog(D_p)_{375nm}$ as a function of seawater temperature. Error bars represent 1σ.

4.3. Surface Bubble Size Distributions

For each experiment, images of the water surface were taken every two

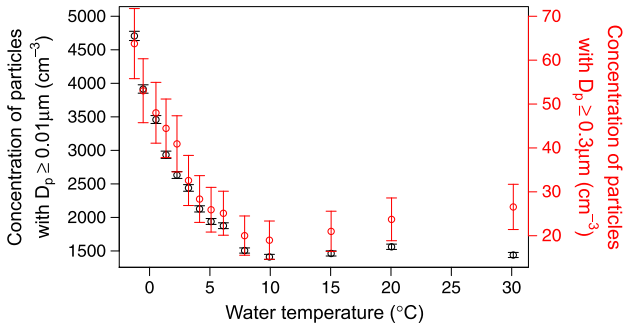

Figure 8. Concentration of particles with $D_p > 0.01\mu$m (black) and $D_p > 0.3\mu$m (red) as a function of seawater temperature. Error bars represent 1σ.

minutes over at least 1.5 h and subsequently analyzed to obtain surface bubble size distributions. Plots of surface bubble size distributions at all of the temperatures investigated are shown in Figure 9. The bubble size distributions are presented in absolute units of bubbles m$^{-2}\mu$m^{-1} radius, that is, the number of bubbles per unit area of water surface per micrometer increment in bubble film radius. This is different from the standard way of reporting bubble size distributions in the oceanographic literature, m$^{-3}\mu$m^{-1} radius, which is based on measured bubble sizes in a volume close to the surface.

In addition to the standard approach of presenting size distribution data on log-log axes, we also present data on semilog axes to better differentiate the differences in the measurements at the five coldest temperatures, where the relative errors are largest. For seawater temperatures below ~4°C, the bubble density increases as the measured bubble film radius decreases. However, at seawater temperatures higher than ~4°C, there appears to be a small mode of bubbles centered around 1 mm to 2 mm, which becomes increasingly prominent as seawater temperature increases. When plotted as the number of bubbles per unit area of water surface per micrometer increment in bubble film radius, the shape of the curves suggests that the maximum bubble density will be located at a bubble film radius somewhat smaller than the detection limit of the method used (bubble film radius = 0.25 mm).

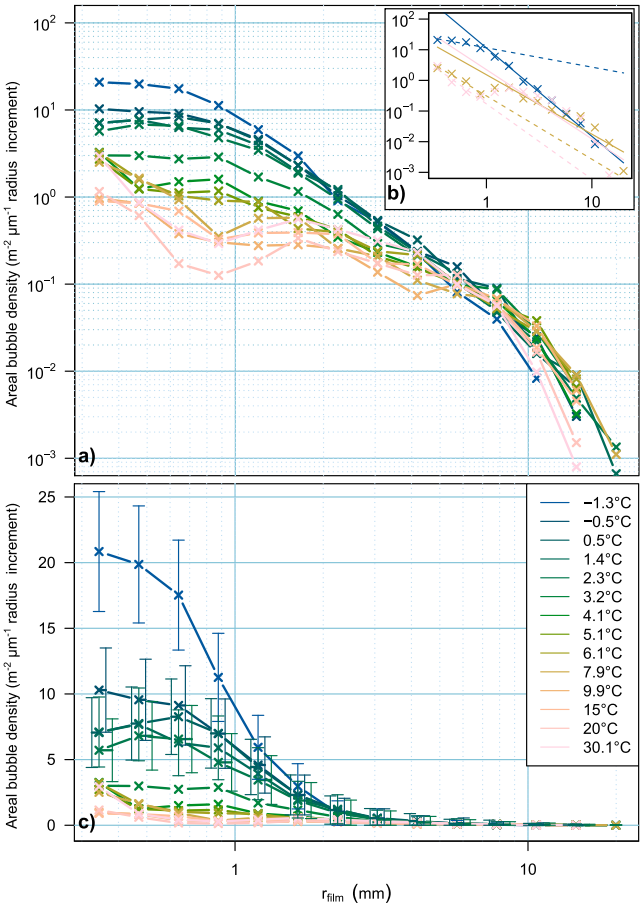

Figure 9. (a) Log-log and (c) semilog areal bubble size distributions as a function of seawater temperature along with error bars (1σ) for the coldest five temperatures (where the errors are largest). In some instances, lines are offset slightly to avoid overlap. (b) Power law fits to the mean size distributions at −1.3°C, 7.9°C, and 30.1°C (see text for details). This panel has the same axis units as Figure 9a.

It appears that the number of bubbles with bubble film radius smaller than 2 mm decreases with increasing seawater temperature. The relative uncertainty in the data is greater at larger bubble sizes because of the smaller number of bubbles. This might explain why the bubble size distributions of bubbles with film radius larger than 2 mm do not appear to be appreciably different across the range of temperatures studied.

Since bubble density in both natural and laboratory breaking waves is often represented as a power law scaling of bubble radius [*Garrett et al.*, 2000; *Deane and Stokes*, 2002], we have attempted to fit power laws to the bubble size distributions obtained at each temperature using different power law coefficients for the bubble film radius regions larger (β) and smaller (α) than 1 mm.

Table 4. Summary of the Bubble Distributions as a Function of Seawater Temperature

T_w	α[a]			β[a]			Mean r_{film}	Maximum r_{film}
(°C)	a	α	R^2 of Fit	b	β	R^2 of Fit	(mm)	(mm)
−1.3	11.6	−0.6	0.73	11.5	−2.9	0.99	0.9	9.9
−0.5	7.0	−0.4	0.78	9.7	−2.7	0.96	1.2	13.2
0.5	7.5	0.01	0.49	9.0	-2.5	0.98	1.3	12.2
1.4	5.8	−0.2	0.52	10.3	−2.8	0.96	1.3	13.0
2.3	5.3	−0.2	0.19	8.1	−2.7	0.98	1.3	17.0
3.2	2.8	−0.1	0.12	3.2	−2.1	0.95	1.8	13.5
4.1	1.2	−0.6	0.03	1.9	−2.0	0.89	2.0	14.0
5.1	0.9	−0.8	0.47	1.5	−1.7	0.92	2.3	13.7
6.1	0.7	−1.3	0.87	1.5	−1.7	0.94	2.2	12.5
7.9	0.3	−2.1	0.95	1.5	−1.9	0.87	2.5	15.4
9.9	0.2	−1.4	0.88	0.6	−1.3	0.81	3.2	12.1
15.0	0.3	−1.0	0.71	1.1	−1.7	0.85	2.7	11.0
20.1	0.1	−2.5	0.93	0.8	−1.7	0.67	3.0	10.9
30.1	0.2	−2.5	0.91	2.2	−2.3	0.76	2.3	10.8

[a]The bubble size distribution at each temperature was fitted with two power laws. The first, fitted in the region $r_{film} < 1$ mm, varies as $a \times r_{film}^{\alpha}$, and the second, fitted in the region $r_{film} > 1$ mm, varies as $b \times r_{film}^{\beta}$.

The inset in Figure 9 shows these fits for seawater temperatures of −1.3°C, 7.9°C and 30.1°C, respectively, while Table 4 details the corresponding exponents and coefficients of determination. The extent with which the power law fits agree with the data for bubbles with film radius smaller than 1 mm is variable ($0.19 < R^2 < 0.95$) and the fits result in exponents (α) ranging from 0 and to −2.5. The fits for bubbles with film radius larger than 1 mm are consistently better ($0.67 < R^2 < 0.99$) and result in exponents (β) which range from −1.3 to −2.9. Figure 10 shows the α and β exponents as a function of seawater temperature. The α exponent shows a tendency to decrease with increasing seawater temperature, while the β exponent shows a tendency to increase with increasing seawater temperature in the range −1.3°C to ∼10°C before leveling off.

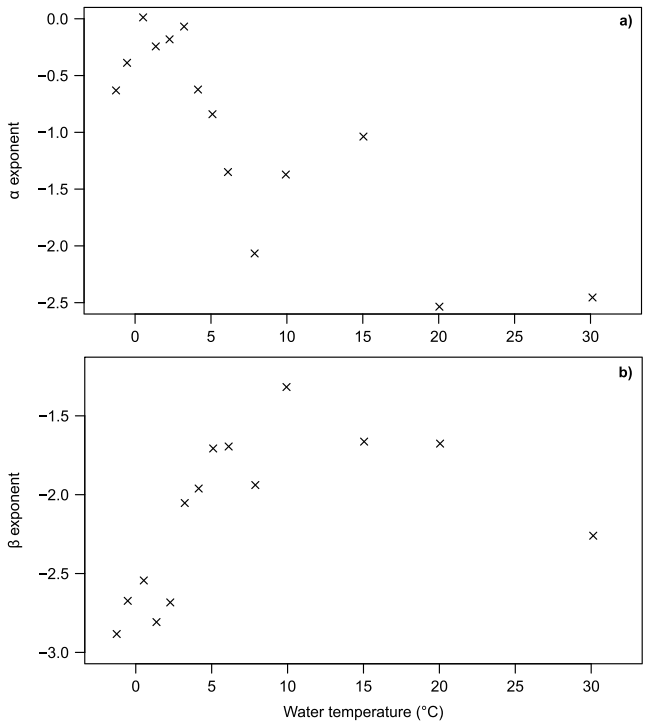

Figure 10. (a) The α exponent of a power law fit to the bubble size distribution (in the form $a \times r_{film}^{\alpha}$) in the region $r_{film} < 1$ mm as a function of seawater temperature. (b) The β exponent of a power law fit to the bubble size distribution (in the form $b \times r_{film}^{\beta}$) in the region $r_{film} > 1$ mm as a function of seawater temperature.

4.4. Total Surface Bubble Concentration

We define the total surface bubble concentration as the total number of bubbles per unit surface area of water. The total surface bubble concentration (bubble film radius > 0.25 mm) at the water surface as a function of seawater temperature is presented in Figure 11. The total surface bubble concentration decreased markedly as the seawater temperature increased up to 10°C. The mean total particle number concentration ($D_p > 0.01\mu$m) as a function of the mean total surface bubble concentration is presented in Figure 12. The data are fitted well by a linear relationship ($R^2 = 0.96$; P-value $= 9.7 \times 10^{-10}$)

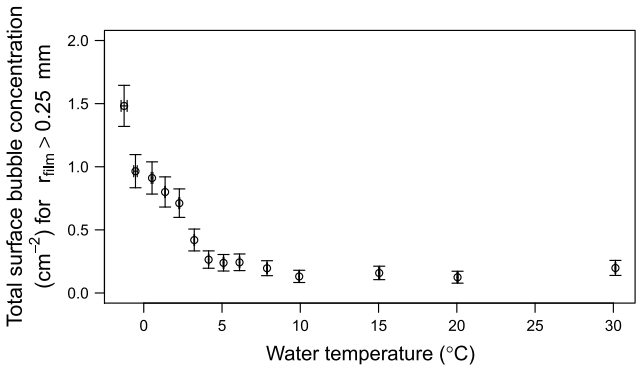

Figure 11. Total surface bubble concentration as a function of seawater temperature. Error bars represent 1σ.

with the total number of particles increasing as the total surface bubble concentration at the water surface increases.

4.5. Air Entrainment

Air entrainment by the plunging jet used in this study was measured across the same range of temperatures as those used to investigate the aerosol and bubble parameters. Figure 13 presents air entrainment (corrected to a standard temperature of 298.15 K and a standard pressure of 1013.25 hPa) as a function of seawater temperature. As the temperature of the artificial seawater increased from ~-1°C to ~30°C, the amount of air entrained decreased by ~35%. The relationship between air entrainment rate and seawater temperature is well represented by a linear relationship ($R^2 = 0.99$; P-value $= 1.7 \times 10^{-13}$).

5. Discussion

5.1. Particle Size Distributions

Our data exhibit a strong decrease in the concentration of the smallest particles (D_p <~1 μm) with increasing seawater temperature (Figure 6). It should be remembered that the number of large particles measured suffers from losses incurred during our efforts to dry the aerosol sufficiently (Figure 2 and section 3.3), but even so, an increase in concentration of the larger particles ($D_p >$ 0.3 μm) with increasing temperature at seawater temperatures above ~10°C is observed. This is consistent with laboratory studies by *Bowyer et al.* [1990] and *Mårtensson et al.* [2003] although there are differences in the particle diameter for which the particle production flux stabilizes or starts to increase with temperature as discussed in section 2.4. There might be several reasons for this difference including the different types of seawater studied, the different methods of air entrainment, and the different aerosol measurement instrumentation used in the three studies (*Bowyer et al.* [1990], *Mårtensson et al.* [2003], and this work).

5.2. Particle Number Concentration

We observed a strongly nonlinear decrease of particle number concentration with increasing seawater temperature in the range from −1.3°C to 9°C (Figure 8). In comparison, the decrease in number concentration of particles of $D_p >$ 0.25μm observed by *Bowyer et al.* [1990] occurred as the seawater temperature was increased from 0°C to 13°C. The only other studies with a high enough temperature resolution in this temperature range to compare with are *Zábori et al.* [2012b], who observed that particle production (all particles with dry diameter larger than 0.01μm) decreased as seawater temperature increased from −1°C to 9.5°C, and *Zábori et al.* [2012a] who observed that particle production decreased as seawater temperature was increased from −1°C to 8.5°C or 9°C, depending on the seawater composition in their experiment.

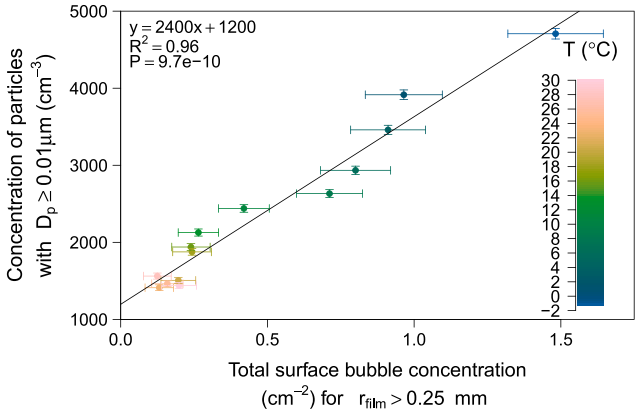

Figure 12. Concentration of particles with $D_p > 0.01\mu$m as a function of the total surface bubble concentration. Error bars represent 1σ.

In the current study, the particle concentration at 9°C is roughly a factor of 3 smaller than at −1.3°C. This is similar to results from the *Bowyer et al.* [1990] study where the particle number concentration (all particles larger than D_p = 0.25μm) at 13°C was also a factor of

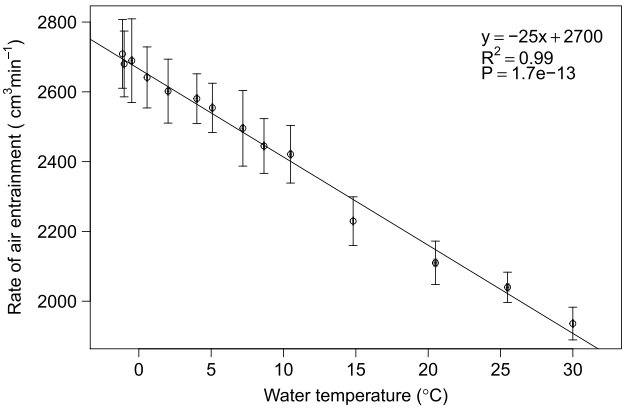

Figure 13. The mean volume of air entrained by the plunging jet as a function of seawater temperature corrected to a standard temperature of 298.15 K and a standard pressure of 1013.25 hPa. Error bars represent 1σ.

3 lower than at 0°C. In contrast to the close agreement of these two studies, *Zábori et al.* [2012a] observed a decrease in particle number concentration by a factor of ~10 as the temperature was increased from −1°C to 9.5°C and *Zábori et al.* [2012b] by a factor ~7 as the temperature was increased from −1°C to 9°C.

The discrepancy between these studies can perhaps be explained by the differences in the experimental setups used. For example, the absolute magnitude of the particle flux likely depends on the amount of air entrained, which in the current study and those of *Zábori et al.* [2012a] and *Zábori et al.* [2012b] was dependent on the characteristics of the plunging jet used (e.g., the jet velocity). It could also be due to the differing organic composition of the seawater used in the different experiments. Another possibility is that the different laboratory setups generated different bubble size distributions due to differences in the characteristics of the air entrainment and that this may have resulted in different particle size distributions. However, if that was the case, then the difference in the absolute magnitude of the particle flux with the same difference in seawater temperature should have remained approximately equal across the different experiments. That the difference in the absolute magnitude of the particle flux is so much larger in the studies of *Zábori et al.* [2012a] and *Zábori et al.* [2012b] when compared to the difference seen in the current study and the study conducted by *Bowyer et al.* [1990] over a similar seawater temperature range suggests that something was fundamentally different about these experiments. What is consistent between these studies is the strong temperature dependence of the total particle number concentration at seawater temperatures below 9°C to 13°C.

5.3. Surface Bubble Size Distributions

The recent discussion of the best method to simulate sea spray aerosol in the laboratory has evolved around comparison of the laboratory and oceanic subsurface bubble spectra. Bubble size distributions generated using the plunging jet (or modifications thereof [e.g., *Stokes et al.*, 2013]) have been suggested to better represent the bubble size distributions of oceanic bubble plumes than bubbles created by air forced through an immersed frit [*Stokes et al.*, 2013]. Sea spray aerosol production is a result of bubbles that burst on the surface, and as mentioned earlier, the bubble plume changes characteristics as it rises to the surface and reaches the air-water interface. In contrast to previous studies, we here focus on the characteristics of the bubble plume at the water surface at different seawater temperatures.

Our measurements of surface bubble spectra generated by a laboratory plunging jet are, to our knowledge, the first of their kind, making direct comparison with previous studies impossible. There are also few measurements of surface bubble spectra or foam generated by oceanic breaking waves in the literature. Those that do exist often use outdated projection techniques which may introduce further error into the analysis [e.g., *Podzimek*, 1984]. Given the dominance of subsurface bubble spectra (density versus bubble radius (r_b)) in the literature, we have plotted our surface bubble size distributions (density versus bubble film radius (r_{film})) alongside measurements of bubble size distributions within whitecaps in two oceanic studies and a laboratory study (Figure 14).

As mentioned in section 4.3, the standard units for bubble size spectra in the oceanographic literature are absolute units of bubbles $m^{-3}\,\mu m^{-1}$ radius increment (right axis, Figure 14); however, our measurements are over the free surface of the water rather than a volume. Therefore, they are presented in absolute units of bubbles $m^{-2}\,\mu m^{-1}$ radius increment (left axis, Figure 14). Comparison of the bubble size spectra, generated by the system used in our study, illustrates that we produce a broad spectrum of bubble sizes, including many bubbles much larger than the Hinze scale [*Deane and Stokes*, 2002]. The Hinze scale is a transition radius occurring at a bubble radius between 0.5 and 1.5 mm in open ocean whitecaps. It represents the

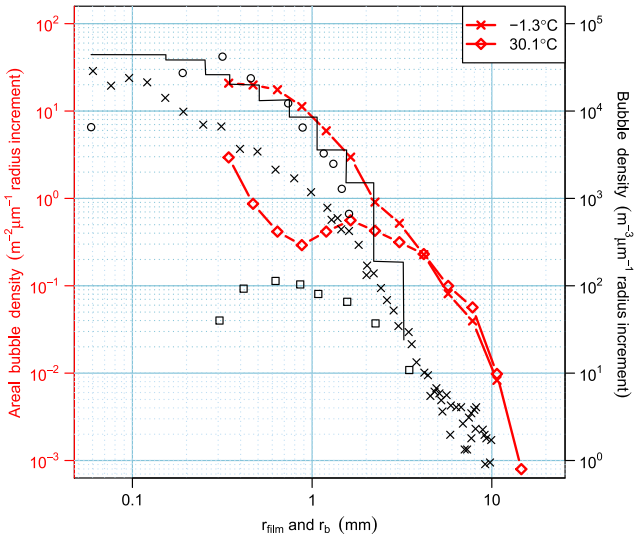

Figure 14. Bubble size distributions (density versus bubble radius (r_b)) in open ocean and laboratory whitecaps (black symbols, right axis) as well as bubble size distributions (density versus bubble film radius (r_{film})) generated at the coldest (crosses) and warmest temperatures (diamonds) investigated during our study (red symbols, left axis). Note the different axes and units. Black squares are *Loewen et al.* [1995], black circles *Bezzabotnov et al.* [1986], solid black line *Cipriano and Blanchard* [1981], and black crosses *Deane and Stokes* [2002].

transition between bubbles stabilized by surface tension (i.e., bubbles smaller than the Hinze scale) and bubbles subject to fragmentation by turbulence (bubbles larger than the Hinze scale) [*Deane and Stokes*, 2002].

The slopes of our measured bubble densities versus bubble film radius appear quite similar to those found in oceanic breaking waves (bubble radius), despite the fact that our data represent floating bubbles rather than rising bubbles. This is interesting considering that the two bubble populations are related through an extra unit of length. It is also interesting to note that the β exponent of the power law fit to the bubble size distribution in the region $r_{film} > 1$mm (Figure 10) increases markedly as the seawater temperature was increased from −1.3°C to ∼10°C before leveling off. This is striking because it is at ∼10°C that the trend of decreasing particle concentration with increasing seawater temperature ceases.

Images of the surface obtained during our experiments clearly show that our surface was always characterized by two-dimensional rafts of bubbles and that the foam layer was never more than a single bubble thick (the expected final result of whitecap foam decay) (Figure 4). This is important given that three-dimensional foams are likely to suppress jet drops originating from bubbles in the lower layers. That the plunging jet used in this study did not produce three-dimensional foams is likely a result of the absence of surfactants in our experiments or a low rate of bubble production resulting from a low jet velocity and thus a low rate of air entrainment. Since real seawater likely contains a variety of organic compounds, many of which are surface active, we recommend that experiments with real seawater or artificial seawater manipulations (e.g., with bacteria or phytoplankton) should image the bubbles at the water surface to ascertain the predisposition of the experimental setup to such effects.

There are clear differences in the bubble spectra obtained at different seawater temperatures (Figure 9). The density of bubbles with bubble film radius smaller than 2 mm decreases markedly between the coldest seawater studied and seawater temperatures of ∼10°C. It is also interesting that a minima in bubble density occurs in bubble spectra (at bubble film radius ∼0.9 mm) obtained from seawater temperatures above ∼10°C; however, it is not clear if this results from a relative increase in bubble density at the smallest sizes of bubbles counted (bubble film radius = 0.25 mm) or at some value higher than this minima (bubble film radius ∼1.6 mm). Given that we observe a slight trend of an increasing number of large particles ($D_p > 0.3$ μm) as seawater temperature increases above 10 °C and that these particles are known to emanate from the smallest bubbles via jet drop production, it seems plausible that the number of bubbles around and below the detection limit of our method may be increasing as the temperature increases from 10°C to 30°C. Once again there are clear parallels with the coincident aerosol measurements; it is at approximately this seawater temperature that the trend of decreasing particle concentration with increasing seawater temperature ceases and at which the trend of increasing concentration of larger particles ($D_p >$∼0.3 μm) with increasing seawater temperature begins.

Qualitatively, the changes observed in our bubble size distributions as the seawater temperature was increased agree with the studies of *Asher and Farley* [1995] and *Slauenwhite and Johnson* [1999] both of which noted decreasing bubble concentrations as seawater temperature was increased.

As to the mechanism behind the observed marked change in bubble spectra at ~10°C observed in our study, we are limited to speculation. Given the changes in viscosity, gas solubility, surface tension, and density of seawater as a function of seawater temperature, the bubble size distribution is likely to be a function of one or more of these parameters.

5.4. Total Surface Bubble Concentration

Since the only variable adjusted during this study was seawater temperature, we are able to consider the total surface bubble concentration in the area of water imaged at high resolution (56 cm^{-2}) as a function of seawater temperature. Given the bubble size spectra presented previously (Figure 9), it is not surprising that the total surface bubble concentration decreases with increasing seawater temperature (Figure 11) up to a seawater temperature of ~10°C. Figure 12 shows the concentration of aerosols produced as a function of the total surface bubble concentration. Since the bubbles are the source of aerosol particles, it seems reasonable that there is also a strong correlation between total particle concentration and the total surface bubble concentration as observed (Figure 12). We note that although these two quantities are linearly related over the area imaged, they are not directly proportional. Indeed, given that there is still a high concentration of particles at a total surface bubble concentration close to 0 (Figure 12), it is likely that many of the particles result from bubbles with $r_{film} < 0.25$ mm, the detection limit of our measurements.

5.5. Air Entrainment

Since the process responsible for bubble generation in the tank is air entrainment by the plunging jet, we have attempted to measure the rate of air entrainment as a function of seawater temperature (Figure 13).

The mechanism of air entrainment depends upon the jet velocity at impact, the fluid properties, the nozzle design, the free-falling jet length, and the jet turbulence. Thus, as we change seawater temperature, while keeping all others parameters constant, we effectively change the fluid properties and the jet turbulence.

It is important to note that plunging jets of a low-viscosity fluid such as seawater are subject to scale effects [*Chanson*, 1997]; therefore, caution should be applied in extending interpretation beyond the system within which the measurements were conducted (see section 3.2). It should also be noted that we applied a rather rudimentary method to obtain estimates of the air entrained, and it cannot be ruled out that our experimental design for measuring air entrainment is not representative for conditions under which the actual experiments were conducted. For example, confined plunging jets, as was the case for our air entrainment measurements, may be inherently different to unconfined plunging jets, such as that deployed during the aerosol/bubble measurements. The action of the jet plunging into a confined volume can generate intense recirculation and consequently higher energy dissipation rates than the same jet in unconfined conditions [*Kiger and Duncan*, 2012].

There are also uncertainties regarding the actual length of the free jet during the air entrainment experiments due to the difficulty in determining the water level in the column at which impingement occurred. This is important since air entrainment has been shown to be a function of the length of the free jet [*Bin*, 1993]. However, since we used a low-pressure-drop method to obtain measurements of the entrained air volume, pressure within the column should have remained constant (at ambient atmospheric pressure) for the duration of the experiments; therefore, we deem it unlikely that the water level in the column changed significantly during the experiments designed to measure air entrainment.

Although very few studies have considered the role of water (or other liquid) temperature on the air entrainment characteristics of plunging jets [*Kiger and Duncan*, 2012], a number of studies have attempted to change the temperature dependent fluid properties (density, viscosity, and surface tension) of the jet in order to observe the effect on air entrainment. Seawater viscosity is strongly temperature dependent, decreasing with increasing seawater temperature from 0.002 Pa s at 0°C to near 0.0009 Pa s at 30°C [*Lewis and Schwartz*, 2004]. The trend observed in our data (Figure 13) of decreasing air entrainment with increasing seawater temperature and thus decreasing seawater viscosity has been observed in a number of other studies. *Kumagai and Endoh* [1982, 1983a, 1983b] determined that the dependence of air entrainment on the liquid viscosity of a plunging jet was complex. When the jet was laminar, air entrainment decreased as liquid viscosity increased; however, when the jet was turbulent, air entrainment was enhanced as liquid viscosity was increased.

El Hammoumi et al. [2002] studied both laminar and turbulent jets and reported results in agreement with these studies. Given that the jet employed during our study was certainly turbulent, to the extent that

the water jet visibly broke into large droplets interspersed with air, our data are also in agreement with these results.

Combining our observations of variation of air entrainment rate (Figure 13), characteristics of surface bubbles (Figures 9 and 11) and particle production (Figure 8) with seawater temperature yields a complex picture where causes and effects are hard to reconcile. Air entrainment increases linearly as seawater temperature decreases, while particle production increases nonlinearly.

Two recent studies of the temperature dependence of air entrainment in hydraulic jumps [*Mortensen*, 2009; *Mortensen et al.*, 2011] also observed decreasing air entrainment with increasing water temperature. The authors postulate that increasing water temperature in the hydraulic jump increased subsurface bubble sizes with the consequence that larger air bubbles led to less breakup of the entrained air, causing less air to be entrained into the hydraulic jump even though the Reynolds and Weber numbers had increased. Given that we observed more small bubbles at the surface at lower seawater temperatures, perhaps the increased air entrainment and particle production at these lower temperatures both result from changes to the bubble size distribution, as postulated by *Mortensen* [2009].

6. Summary and Conclusions

We have attempted to reconcile previous observations on the effects of seawater temperature on aerosol particle production in laboratory sea spray aerosol studies. In addition, we have for the first time measured the density of bubbles at the water surface as a function of seawater temperature. Aerosol particles were generated by water impingement using a continuous plunging jet in a large-scale temperature controlled sea spray simulator. Air entrainment rate by the plunging jet, surface bubble size distributions, and size distributions of the produced aerosol particles were studied as a function of seawater temperature over the range −1.3°C to 30.1°C.

We observed that air entrainment decreased across this seawater temperature range, perhaps due to increased turbulence in the jet prior to impingement or as a result of modification of the processes involved in the fragmentation of the air entrained as the fluid properties (density, viscosity, and surface tension) change with temperature. The latter speculation is supported by our observations of surface bubble spectra, which change significantly as a function of seawater temperature with a large decrease in the density of surface bubbles with bubble film radius smaller than 2 mm as seawater temperature increases.

The particle size distributions obtained during the study support trends identified in previous studies, that is, large decreases in the number concentration of particles with dry diameter less than 1 μm as seawater temperature increases up to ~9°C and small increases in the concentration of larger ($D_p > 1\mu$m) particles thereafter with increasing seawater temperature. The total number concentration of particles scaled linearly with the total surface bubble concentration suggesting that the dramatic increase in number concentration of bubbles with film radius less than 2 mm at lower temperatures is responsible for the observed increase in number concentration of particles less than 1μm dry diameter. The simultaneous change in bubble size spectra and total particle concentration at a seawater temperature around ~10°C also suggests that the changing bubble size distribution drives the changes in aerosol concentrations observed.

A pertinent question arising as a result of this study is whether our findings are relevant outside of the laboratory. Our results showing decreased air entrainment by a continuous plunging jet coincident with decreased numbers of bubbles with film radius $<$ 2 mm and decreased total particle production with increasing seawater temperature leave the validity of using such continuous systems to model the intermittency of wave breaking open to question. Is the continuous nature of the plunging jet used in this study responsible for the strong temperature dependence of bubble film radius and consequent increase in particle production? Or does the mechanism responsible also occur in intermittent systems such as ocean breaking waves? Such questions provide an important focus for future research since our results, if applicable to the open oceans, imply that submicron aerosol production would be greater at high latitudes (due to increased bubble density at lower seawater temperatures) than at lower latitudes at a given air entrainment (other factors notwithstanding). This is an important finding given that large expanses of cold, open water are likely to arise in the Arctic following the ice melt predicted to occur in the next ~50 years. Both this temperature effect and the coincident decrease in ocean surface salinity might be important for the sea spray aerosol flux in the region in the coming years.

Appendix A: List of Symbols

D_p dry diameter of SSA particles.
γ_{sw} surface tension of seawater.
μ_{sw} dynamic viscosity of seawater.
N_{film} mean number of film drops produced per bubble.
N_{jet} mean number of jet drops produced per bubble.
P air pressure.
r_b volume equivalent bubble radius, defined such that the volume of the bubble is equal to $(4\pi/3)\, r_b^3$.
r_{film} radius of the circle formed by the intersection of the bubble film or cap with the water surface.
ρ_{sw} density of seawater.
R^2 coefficient of determination.
S_A absolute salinity.
T air temperature.
T_{sw} seawater temperature.
U mean wind speed at 10 m above the sea surface.
V_b rise velocity of bubbles in seawater.
W oceanic whitecap fraction or ratio.

Acknowledgments
Our work was supported by the Swedish Research Council (Vetenskapsrådet), the Carlsberg Foundation (grant 2009_01_0515), and the Nordic Center of Excellence on Cryosphere-Atmosphere (CRAICC). The authors would like to thank Sarah Howald for her contribution to the laboratory experiments conducted during this study, Hubert Chanson and Ernie Lewis for their helpful suggestions during the preparation of this manuscript, and two anonymous reviewers for their detailed comments. The data from this study are available from the authors upon request.

References

Alofs, D. J., and P. Balakumar (1982), Inversion to obtain aerosol size distributions from measurements with a differential mobility analyzer, *J. Aerosol Sci.*, *4736*, 513–527.
Asher, W. E., and P. J. Farley (1995), Phasedoppler anemometer measurement of bubble concentrations in laboratory-simulated breaking waves, *J. Geophys. Res.*, *100*, 7045–7056, doi:10.1029/95JC00068.
Bezzabotnov, V. S., R. S. Bortkovskii, and D. F. Timanovskii (1986), On the structure of the two-phase medium generated at wind-wave breaking, *Izv. Akad. Nauk SSSR, Phys. Atmos. Ocean*, *22*, 1186–1193.
Biń, A. K. (1993), Gas entrainment by plunging liquid jets, *Chem. Eng. Sci.*, *48*(21), 3585–3630, doi:10.1016/0009-2509(93)81019-R.
Blanchard, D. C. (1963), The electrification of the atmosphere by particles from bubbles in the sea, *Prog. Oceanogr.*, *1*, 73–112, doi:10.1016/0079-6611(63)90004-1.
Bortkovskii, R. S. (1987a), Spatial and temporal characteristics of white horses and spindrift generated from wind wave collapse, *Russ. Meteorol. Hydrol.*, *5*, 68–75.
Bortkovskii, R. S. (1987b), *AirSea Exchange of Heat and Moisture During Storms*, Reidel, Dordrecht.
Bortkovskii, R. S. (1997), On the influence of water temperature on the ocean-surface state and transfer processes, *Izv. Atmos. Oceanic Phys.*, *33*, 242–248.
Bortkovskii, R. S., and V. A. Novak (1993), Statistical dependencies of sea state characteristics on water temperature and wind-wave age, *J. Mar. Syst.*, *4*, 161–169.
Bowyer, P. A., D. K. Woolf, and E. C. Monahan (1990), Temperature dependence of the charge and aerosol production associated with a breaking wave in a whitecap simulation tank, *J. Geophys. Res.*, *95*, 5313–5319.
Chanson, H. (1997), *Air Bubble Entrainment in Free-Surface Turbulent Shear Flows*, Academic Press, London.
Chanson, H., S. Aoki, and A. Hoque (2006), Bubble entrainment and dispersion in plunging jet flows: Freshwater vs. seawater, *J. Coastal Res.*, *22*, 664–677.
Cipriano, R. J., and D. Blanchard (1981), Bubble and aerosol spectra produced by a laboratory breaking wave, *J. Geophys. Res.*, *86*, 8085–8092.
Cummings, P. D., and H. Chanson (1999), An experimental study of individual air bubble entrainment at a planar plunging jet, *Chem. Eng. Res. Des.*, *77*, 159–164.
Deane, G. B., and M. D. Stokes (2002), Scale dependence of bubble creation mechanisms in breaking waves, *Nature*, *418*, 839–844.
El Hammoumi, M., J. L. Achard, and L. Davoust (2002), Measurements of air entrainment by vertical plunging liquid jets, *Exp. Fluids*, *32*, 624–638.
Exton, H., J. Latham, P. Park, M. Smith, and R. Allan (1986), The production and dispersal of maritime aerosol, in *Oceanic Whitecaps, Oceanographic Sciences Library*, vol. 2, edited by E. Monahan and G. Niocaill, pp. 175–193, Springer, London.
Garrett, C., M. Li, and D. Farmer (2000), The connection between bubble size spectra and energy dissipation rates in the upper ocean, *J. Phys. Oceanogr.*, *30*, 2163–2171.
Hayami, S., and Y. Toba (1958), Drop production by bursting of air bubble on the sea surface. 1. Experiments at still sea water surface, *J. Oceanogr. Soc. Jpn.*, *14*, 145–150.
Heim, M., B. J. Mullins, H. Umhauer, and G. Kasper (2008), Performance evaluation of three optical particle counters with an efficient multimodal calibration method, *J. Aerosol Sci.*, *39*, 1019–1031.
Hultin, K. A. H., E. D. Nilsson, R. Krejci, M. Mårtensson, E. M. Ehn, A. Hagström, and G. de Leeuw (2010), In situ laboratory sea spray production during the marine aerosol production 2006 cruise on the northeastern atlantic ocean, *J. Geophys. Res.*, *115*, D06201, doi:10.1029/2009JD012522.
Hultin, K. A. H., R. Krejci, J. Pinhassi, L. Gomez-Consarnau, E. M. Mårtensson, A. Hagström, and E. D. Nilsson (2011), Aerosol and bacterial emissions from baltic seawater, *Atmos. Res.*, *99*, 1–14, doi:10.1016/j.atmosres.2010.08.018.
Kandlikar, M., and G. Ramachandran (1999), Inverse methods for analysing aerosol spectrometer measurements: A critical review, *J. Aerosol Sci.*, *30*, 413–437.
Kiger, K. T., and J. H. Duncan (2012), Air-entrainment mechanisms in plunging jets and breaking waves, *Annu. Rev. Fluid Mech.*, *44*(1), 563–596.
Kumagai, M., and K. Endoh (1982), Effects of kinetic viscosity and surface tension on gas entrainment rate of an impacting liquid jet, *J. Chem. Eng. Jpn.*, *15*, 427–433.

Kumagai, M., and K. Endoh (1983a), A note on the relationship between gas entrainment curve and its starting velocity, *J. Chem. Eng. Jpn.*, *16*, 74–75.
Kumagai, M., and K. Endoh (1983b), Mean residence time and gas hold-up of entrained gas by an impinging water jet, *J. Chem. Eng. Jpn.*, *16*, 357–363.
Lessard, R. R., and S. A. Zieminski (1971), Bubble coalescence and gas transfer in aqueous electrolytic solutions, *Ind. Eng. Chem.*, *10*(2), 260–269.
Lewis, E. R., and S. E. Schwartz (2004), *Sea Salt Aerosol Production: Mechanisms, Methods, Measurements and Models—A Critical Review, Geophys. Monogr.*, vol. 152, AGU, Washington, D. C.
Loewen, M. R., M. A. O'Dor, and M. G. Skafel (1995), Laboratory measurements of bubble size distributions beneath breaking waves, in *Air-Sea Gas Transfer, Third International Symposium on Air-Water Gas Transfer*, edited by B. Jahne and E. C. Monahan, pp. 337–345, AEON Verlag & Studio, Germany.
Mårtensson, E. M., E. D. Nilsson, G. de Leeuw, L. H. Cohen, and H. C. Hansson (2003), Laboratory simulations and parameterization of the primary marine aerosol production, *J. Geophys. Res.*, *108*(D9), 4297, doi:10.1029/2002JD002263.
Miyake, Y., and T. Abe (1948), A study on the foaming of sea water. Part 1, *J. Mar. Res.*, *7*, 67–73.
Monahan, E. C., and G. Mac Niocaill (1986), *Oceanic Whitecaps and Their Role in Air-Sea Exchange Processes*, Reidel, Dordrecht.
Monahan, E. C., and I. O'Muircheartaigh (1980), Optimal power-law description of oceanic whitecap coverage dependence on wind speed, *J. Phys. Oceanogr.*, *10*, 2094–2099.
Monahan, E. C., and I. O'Muircheartaigh (1986), Whitecap and the passive remote sensing of the ocean surface, *Int. J. Remote Sens.*, *7*, 627–642.
Monahan, E. C., D. E. Spiel, and K. L. Davidson (1982), Whitecap aerosol productivity deduced from simulation tank measurements, *J. Geophys. Res.*, *87*, 8898–8904.
Monahan, E. C., C. W. Fairall, K. L. Davidson, and P. C. Boyle (1983), Observed inter-relations between 10 m winds, ocean white caps and marine aerosols, *Q. J. R. Meteorolog. Soc.*, *109*, 379–392.
Mortensen, J. D. (2009), Factors affecting air entrainment of hydraulic jumps within closed conduits, PhD thesis, Utah State Univ., Logan.
Mortensen, J. D., S. L. Barfuss, and M. C. Johnson (2011), Scale effects of air entrained by hydraulic jumps within closed conduits, *J. Hydraul. Res.*, *49*, 90–95.
Najjar, R. G., and R. F. Keeling (1997), Analysis of the mean annual cycle of the dissolved oxygen anomaly in the World Ocean, *J. Mar. Res.*, *55*, 117–151.
Newitt, D. M., N. Dombrowski, and F. H. Knelman (1954), Liquid entrainment. 1. The mechanism of drop formation from gas or vapour bubbles, *Trans. Inst. Chem. Eng. J.*, *32*, 244–261.
Nilsson, E. D., U. Rannik, E. Swietlicki, C. Leck, P. P. Aalto, J. Zhou, and M. Norman (2001), Turbulent aerosol fluxes over the Arctic Ocean: 2. Wind-driven sources from the sea, *J. Geophys. Res.*, *106*, 32,139–32,154, doi:10.1029/2000JD900747.
O'Dowd, C. D., and M. H. Smith (1993), Physicochemical properties of aerosols over the northeast Atlantic: Evidence for wind-speed-related submicron sea-salt aerosol production, *J. Geophys. Res.*, *98*, 1137–1149.
Podzimek, J. (1984), Size spectra of bubbles in the foam patches and of sea salt nuclei over the surf zone, *Tellus B*, *36B*(3), 192–202, doi:10.1111/j.1600-0889.1984.tb00241.x.
Pounder, C. (1986), *Oceanic Whitecaps and Their Role in Air–Sea Exchange Processes,* chap. Sodium chloride and water temperature effects on bubbles, p. 278, D. Reidal, Hingham, Mass.
Schneider, C. A., W. S. Rasband, and K. W. Eliceiri (2012), NIH image to imageJ: 25 years of image analysis, *Nat. Methods*, *9*, 671–675.
Sellegri, K., C. D. O'Dowd, Y. J. Yoon, S. G. Jennings, and G. de Leeuw (2006), Surfactants and submicron sea spray generation, *J. Geophys. Res.*, *111*, D22215, doi:10.1029/2005JD006658.
Sharqawy, M. H., J. H. Lienhard, and S. M. Zubair (2010), Thermophysical properties of seawater: A review of existing correlations and data, *Desalin. Water Treat.*, *16*, 354–380.
Slauenwhite, D. E., and B. D. Johnson (1999), Bubble shattering: Differences in bubble formation in fresh water and seawater, *J. Geophys. Res.*, *104*(C2), 3265–3275.
Stagonas, D., D. Warbrick, G. Muller, and D. Magagna (2011), Surface tension effects on energy dissipation by small scale, experimental breaking waves, *Coastal Eng.*, *58*, 826–836.
Stokes, M. D., G. B. Deane, K. Prather, T. H. Bertram, M. J. Ruppel, O. S. Ryder, J. M. Brady, and D. Zhao (2013), A marine aerosol reference tank system as a breaking wave analogue for the production of foam and sea-spray aerosols, *Atmos. Meas. Tech.*, *6*, 1085–1094.
Stramska, M., and T. Petelski (2003), Observations of oceanic whitecaps in the north polar waters of the Atlantic, *J. Geophys. Res.*, *108*(C3), 3086, doi:10.1029/2002JC001321.
Stramska, M., R. Marks, and E. C. Monahan (1990), Bubble-mediated aerosol production as a consequence of wave breaking in supersaturated (hyperoxic) seawater, *Journal of Geophys. Res.*, *95*(C10), 18281–18288.
Thorpe, S. A., P. Bowyer, and D. K. Woolf (1992), Some factors affecting the size distributions of oceanic bubbles, *J. Phys. Oceanogr.*, *22*, 382–389.
Twardowski, M. S., J. M. Sullivan, P. L. Donaghay, and J. R. V. Zaneveld (1999), Microscale quantification of the absorption by dissolved and particulate material in coastal waters with an ac-9, *J. Atmos. Oceanic Technol.*, *16*, 691–707.
von der Weiden, S. L., F. Drewnick, and S. Borrman (2009), Particle loss calculator a new software tool for the assessment of the performance of aerosol inlet systems, *Atmos. Meas. Tech.*, *2*, 479–494.
Wiedensohler, A. (1988), An approximation of the bipolar charge distribution for particles in the sub micron size range, *J. Aerosol Sci.*, *19*, 387–389.
Woodcock, A. H. (1953), Salt nuclei in marine air as a function of altitude and wind force, *J. Meteorol.*, *10*, 362–371.
Woolf, D. K., and E. C. Monahan (1988), Laboratory investigations of the influence on marine aerosol production of the interaction of oceanic whitecaps and surface-active material, in *Aerosol and Climate*, edited by P. V. Hobbs and M. P. McCormack, pp. 1–8, A. Deepak, Hampton, Va.
Woolf, D. K., P. A. Bowyer, and E. C. Monahan (1987), Discriminating between the film drops and jet drops produced by a simulated whitecap, *J. Geophys. Res.*, *92*(C5), 5142–5150, doi:10.1029/JC092iC05p05142.
Wu, J. (1979), Oceanic whitecaps and sea state, *J. Phys. Oceanogr.*, *9*, 1064–1068.
Wu, J. (1988), Bubbles in the near-surface ocean: A general description, *J. Geophys. Res.*, *93*, 587–590.
Zábori, J., R. Krejci, A. M. L. Ekman, E. M. Mårtensson, J. Ström, G. de Leeuw, and E. D. Nilsson (2012a), Wintertime Arctic Ocean sea water properties and primary marine aerosol concentrations, *Atmos. Chem. Phys.*, *12*, 10,405–10,421.
Zábori, J., M. Matisāns, R. Krejci, E. D. Nilsson, and J. Ström (2012b), Artificial primary marine aerosol production: A laboratory study with varying water temperature, salinity and succinic acid concentration, *Atmos. Chem. Phys.*, *12*, 10,709–10,724.
Zábori, J., R. Krejci, J. Ström, P. Vaattovaara, A. M. L. Ekman, M. E. Salter, E. M. Mårtensson, and E. D. Nilsson (2013), Comparison between summertime and wintertime arctic ocean primary marine aerosol properties, *Atmos. Chem. Phys.*, *13*, 4783–4799.